UNIVERSITY OF BIRMINGHAM
University of Birmingham Research at Birmingham

Dynamic culture substrates that mimic the topography of the epidermal-dermal junction

Helling, Ayelen; Viswanathan, Priyalakshmi; Cheliotis, Katerina; Mobasseri, Seyedeh Atefeh; Yang, Ying; El Haj, Alicia J; Watt, Fiona M

DOI:
10.1089/ten.TEA.2018.0125

License:
Other (please specify with Rights Statement)

Document Version
Peer reviewed version

Citation for published version (Harvard):
Helling, A, Viswanathan, P, Cheliotis, K, Mobasseri, SA, Yang, Y, El Haj, AJ & Watt, FM 2018, 'Dynamic culture substrates that mimic the topography of the epidermal-dermal junction', *Tissue Engineering Part A*. https://doi.org/10.1089/ten.TEA.2018.0125

Link to publication on Research at Birmingham portal

Publisher Rights Statement:
Checked for eligibility: 16/10/2018

Final publication is available from Mary Ann Liebert, Inc., publishers http://dx.doi.org/10.1089/ten.TEA.2018.0125

General rights
Unless a licence is specified above, all rights (including copyright and moral rights) in this document are retained by the authors and/or the copyright holders. The express permission of the copyright holder must be obtained for any use of this material other than for purposes permitted by law.

•Users may freely distribute the URL that is used to identify this publication.
•Users may download and/or print one copy of the publication from the University of Birmingham research portal for the purpose of private study or non-commercial research.
•User may use extracts from the document in line with the concept of 'fair dealing' under the Copyright, Designs and Patents Act 1988 (?)
•Users may not further distribute the material nor use it for the purposes of commercial gain.

Where a licence is displayed above, please note the terms and conditions of the licence govern your use of this document.

When citing, please reference the published version.

Take down policy
While the University of Birmingham exercises care and attention in making items available there are rare occasions when an item has been uploaded in error or has been deemed to be commercially or otherwise sensitive.

If you believe that this is the case for this document, please contact UBIRA@lists.bham.ac.uk providing details and we will remove access to the work immediately and investigate.

Download date: 24. Apr. 2024

Response of human epidermal keratinocytes to dynamic substrates that mimic the topography of the epidermal-dermal junction

Ayelen L. Helling[a], Priyalakshmi Viswanathan[a], Katerina Cheliotis[a], Seyedeh Atefeh Mobasseri[a], Ying Yang[b], Alicia J. El Haj[b], Fiona M. Watt[a]

[a] Center for Stem Cells and Regenerative Medicine, King's College London, 28th Floor, Tower Wing, Guy's Hospital, Great maze Pond, London SE1 9RT, UK

[b] Institute for Science & Technology in Medicine Keele University Thornburrow Drive, Hartshill Stoke-on-Trent, ST4 7QB United Kingdom

Corresponding author: Fiona.watt@kcl.ac.uk; Tel: +44 20 7188 5608

Abstract

The junction between the epidermal and dermal layers of human skin undulates, the width and depth of the undulations varying with age and disease. We previously showed that when primary human epidermal keratinocytes are seeded on collagen-coated undulating static Polydimethylsiloxan (PDMS) elastomer substrates, the stem cells, differentiated cells and proliferating cells become patterned in response to cues from the underlying substrate. To investigate how patterning occurs over time, we have now created a dynamic model, in which a collagen-coated PLGA membrane is placed over a polyimide sheet containing circular holes, differing in diameter and the distance between them. When a vacuum is applied the membrane is induced to undulate, the heights of the undulations depending on the pressure applied and the size of the holes. We observed clustering of cells with high levels of β1 integrin expression, a stem cell marker, in the base of the undulations within 48h of applying the vacuum. Differentiating, involucrin-positive cells did not cluster; however, there was clustering of cells with high E-cadherin expression and nuclear YAP. Rho kinase inhibition resulted in loss of clustering, implicating a role for Rho family members in the process.

Keywords: human epidermal-dermal junction**,** dynamic substrate, topography, keratinocytes**,** stem cells

1. Introduction

Mammalian skin is a complex organ that consists of two major layers, the epidermis and the dermis, separated by a basement membrane that is rich in type IV collagen and laminin [1]. The structure of the epidermal-dermal junction in human skin is not flat but undulates, forming a pattern of alternating rete ridges, where the epidermis projects more deeply into the dermis, and dermal papillae, where the dermis comes closest to the skin surface [2]. The depth and width of the rete ridges vary with age and body site, and are increased in the inflammatory skin disease such as psoriasis [3–8].

Stem cells are located in the human epidermal basal layer [9,10] and occupy specific locations relative to the epidermal-dermal junction, in most body sites clustering on the tops of the dermal papillae [9,11,12]. Expression of several cell surface markers is enriched in human epidermal stem cells, including β1-integrin receptors, Lrig1, CD46, MCSP and Delta-like 1.

Previous studies have that demonstrated stem cell fate is regulated by a combination of intrinsic (genetic and epigenetic) and extrinsic signals [1,13], such as soluble factors, cell-cell contact, ECM protein interactions and tissue topography. To mimic different components of the extracellular environment, a number of approaches have been taken, such as co-culture of keratinocytes and dermal fibroblasts on biomaterials, including collagen gels [14], which act as scaffolds for cell growth and also facilitate cell-cell interactions. Other approaches include culture on de-epidermised acellular human dermal matrices [15], self-assembled living sheets made with human fibroblasts and keratinocytes [16], and bioprinted cell-laden hydrogels [17]. However, these models fail to mimic the undulating epidermal-dermal junction. To overcome this limitation several other models [18–20] have been developed. Undulations have been created using static topographies through microfabrication of dermal-epidermal regeneration matrices (μDERMs), for example via fabrication of patterned Polydimethylsiloxan (PDMS) substrates or micro-topographies using photolithography followed by the production of collagen-GAG templates [19].

Using a panel of undulating collagen-coated PDMS substrates [18] that differ in diameter, height and centre-to-centre spacing, we have recently shown that topography is sufficient to direct the formation of β1 integrin bright stem cell clusters on the tops of the features. In

addition, we found that separate topographical cues determined the locations of stem cells, involucrin-positive differentiated cells, and proliferating cells. This prompted us to develop a platform in which we could change topography from flat to undulating in order to measure dynamic cell responses. By simultaneously creating multiple topographies within a single device, we can begin to understand the effect of ageing and other changes on stem cell behaviour.

2. Materials and Methods

2.1. Membrane preparation

Poly(D,L-lactide) (PLA, average Mw 75,000-120,000, ref P1691) and Poly(D,L-lactide-co-glycolide) (PLGA, average Mw 50,000-75,000, ref 430471) were purchased from Aldrich–Sigma. Dichloromethane (DCM, anhydrous, ≥99.8% ref 270997) was purchased from Aldrich–Sigma and used as a solvent to prepare the PLA and PLGA membranes.

PLA was dissolved in DCM in a 5 w/v% and PLGA in a 2 w/v%, using the formula:

$$w/_v\,\% = {mass\ of\ polymer\ (g)}\Big/{volume\ solvent\ (ml)} \times 100 \qquad (1)$$

The concentrations were chosen based on the lowest amount of polymer able to form an elastic thin membrane which will deform under vacuum without collapsing. The solution was made in a glass vial and gently agitated using a magnet stirrer for approximately one hour. After complete dissolution, 7ml of the solution was placed on a 13.5 cm diameter glass petri dish and covered with a lid to guarantee slow evaporation of the solvent at room temperature for 48 hours inside the fume hood. Samples were then sterilised by covering the surface with 70% Ethanol for 30min at room temperature. Finally, membranes were collagen coated using 50 μg/ml of collagen type I (Corning Ref 354236) in PBS for 2 hours at 37^0C.

2.2. Differential Scanning Calorimeter (DSC)

The melting point of the two membranes (PLGA and PLA) was measured using a Differential Scanning Calorimeter (DSC) -Mettler Toledo DSC822e Calorimeter. 3 samples for each polymer were analysed. Sample size was 10 ± 1mg.

2.3. Uniaxial tensile test

The tensile strength of the membranes was measure using uniaxial tensile test - Electro force Model 3200 testing machine (BOSE). The samples were cut according to the ASTM D882

Tensile Strength properties of thin plastic films (film less than 1 mm thick, in a ratio 2:1; 3:0.5 inch). The samples were 10 mm x 30 mm in dimension, tested with a maximum load of 22.2 N and a rate of 0.05 mm/sec.

2.4. Template design

Three topographies were designed using the software AutoCad Autodesk 2016. The topographies were distributed according to the shape of a 12 well cell culture plate to cover surfaces of 1cm by 1cm. Each of the three topographies and a flat control were arranged in triplicate. The dimensions that differed between topographies were the diameters of the drilled holes and the distance between holes. The first topography consisted of drilled holes with a diameter of 100 μm and a distance between holes of 150 μm. The second topography consisted of drilled holes with a diameter of 100 μm and inter-hole distance of 200 μm. The third topography had holes of 200 μm in diameter and a distance of 200 μm between holes.
The template material selected was a 500 μm thick polyimide sheet (Cirlex from GoodFellow), which has good mechanical properties and yet is thin enough for laser drilling. Laser drilling requires a small ratio diameter of drilling: sheet thickness, because the drilled holes become conical if the thickness is too high.

2.5. Rig design

The rig was designed using AutoCad Autodesk 2016 and fabricated with transparent acrylic. It was based on the dimensions of a 12 cell culture well plate and composed of three individual parts that are assembled together and secured with screws. The rig has two barbed fittings to connect the pipe that is attached to the vacuum pump (SAM 18, MGE) that generates the force to deform the culture membrane. The manufacturing process was carried out by the Department of Clinical Technology Mechanical Workshop Activity of the University Hospital of North Midlands NHS Trust.

2.6. Scanning electron microscopy (SEM)

SEM was used to evaluate the deformation of membrane in presence of vacuum. In order to fabricate the samples for SEM, PDMS was added on the membrane while the vacuum was running. Following complete curing, PDMS was peeled from the membrane, creating a replica of the patterns of the membrane. Samples were coated with gold sputter (4 nm thickness) and imaged with SEM using JEOL NeoScope JCM 6000Plus.

2.7. Culture of human keratinocytes

Neonatal human foreskin keratinocytes were cultured on a mitotically inactivated feeder layer comprising the J2 clone of 3T3 cells. As described previously [18] the medium comprised 1 part Ham's F12, 3 parts Dulbecco's modified eagle medium (DMEM), 10^{-4} M adenine, 10% (v/v) fetal bovine serum (FBS), 0.5 μg ml^{-1} hydrocortisone, 5 μg ml^{-1} insulin, 10^{-10} M cholera toxin and 10 ng ml^{-1} EGF (complete FAD medium). Keratinocytes were seeded onto PLA and PGLA membranes at a density of 100,000 cells/cm^2 overnight in complete Keratinocyte Serum Free Medium (KSFM; Gibco), and then transferred for 48 hours to complete FAD medium at 37^0C and 5% CO_2. No vacuum pressure was applied to the rig during the first 20 min in FAD medium. Following this, constant vacuum pressure was applied through the rig, deforming the membrane on which keratinocytes were growing**.**

2.8. Immunolabelling and confocal microscopy

Cells were simultaneously fixed and permeabilised in 4% paraformaldehyde (PFA) and 0.2% Triton-X 100 (Sigma) for 15 minutes, at room temperature. Afterwards they were blocked for 1 h in blocking buffer (10% fetal bovine serum, 0.25% gelatin from cold water fish skin (Sigma) in PBS) at room temperature, incubated with primary antibodies diluted in blocking buffer for 1 h at room temperature or overnight at 4°C, and incubated with Alexafluor (488 and 555)-conjugated secondary antibodies diluted in PBS for 1 h at room temperature. Samples were mounted using mounting media with DAPI (ProLong Gold antifade reagent with DAPI, Invitogen). The following primary antibodies were used: P5D2 (mouse monoclonal anti-β1 integrin; dilution of 1:500; prepared in-house), SY7 (mouse monoclonal anti-involucrin; dilution of 1:1000; prepared in-house); HECD-1 (mouse monoclonal anti-E-cadherin; dilution of 1:1000; prepared in-house); anti-YAP (rabbit; dilution of 1:200; Cell Signalling). Samples were visualised using a Nikon A1 Scanning Confocal Upright microscope.

2.9. Statistical analysis

All values are represented as mean ± standard deviation. Experiments were performed in triplicate. Extra information is shown in the correspondent figure legend. Statistical analysis was carried out using GraphPad Prism 7.0 (GraphPad Software Inc., USA). All data were analysed by one or two factor ANOVA tests. The statistical significance were set at $*P < 0.05$, $**P < 0.01$, $***P < 0.001$ and $****P \leq 0.0001$.

3. Results

3.1. *Membrane characterisation*

PLA and PLGA membranes have been used extensively to support the growth of cultured cells and are translucent, enabling cells to be visualised by light microscopy [21,22]. The polymer concentration of each membrane was chosen based on the minimum concentration that could create an elastic thin membrane that would deform under vacuum pressure without collapsing: 2% (w/v) PLGA and 5 % (w/v) PLA. We therefore compared their thickness and mechanical properties with a view to selecting one as the material for the dynamic substrate. The thickness of the membranes was measured using a digital micrometre (Fig. 1.A, B). We also subjected the membranes to a uniaxial tensile test (Fig. 1C) and measured the melting point using DSC (Fig. 1D). Based on these results, PLGA was chosen over PLA because of its lower thickness and higher elasticity.

3.2. *Template design*

The template for deforming the PGLA membrane was designed using AutoCad software (Fig. 2A) and fabricated by laser drilling a 500 μm thick polyimide sheet (Fig. 2B). The dimensions of each feature were selected based upon previous studies elucidating epidermal-dermal junction topographies in young and aged skin [5]. Three topographies were designed, each of which covered the area of an individual well of a 12 well plate. We also included a fourth topography with no holes, to serve as a flat membrane control. Each topography was reproduced three times in the template, so that within a single experimental run we could compare triplicate cultures exposed to each topography (Fig. 2B-E). As shown in Fig. 2C-E, there was excellent uniformity in the size and patterning of the holes.

3.3. *Rig design and assembly*

The PLGA membrane and template were assembled in a rig made from transparent acrylic (Fig. 3A-D; Supplemental Movie 1). Then a vacuum was applied through two tubes coming from both sides of the rig and connecting to a vacuum pump (Fig. 3E). The pressure from the vacuum drew the membrane through the template, creating invaginations varying in depth and spacing according to topography and applied vacuum pressure (Fig. 4).

To quantify the degree of membrane deformation achieved, PDMS was poured on top of the deformed membrane and then left to cure, as described previously [18], creating an imprinted

stamp of the deformed membrane. The PDMS stamps were imaged using SEM and the images were analysed using ImageJ. Vacuum pressures of 10 kPa, 15 kPa and 20 kPa were used to deform the membrane. Quantitative analysis confirmed that an increase in vacuum pressure correlated with an increased depth of membrane topographies (Fig. 4). Under 15 kPa and 20 kPa (Fig. 4B, C) vacuum pressures, there was a statistically significant difference in the deformation of topography 3 compared topographies 1 and 2. Regardless of topography there was a statistical difference between the deformation due to 20 kPa and the other two vacuum pressures (figures 4D, 4E, 4F). For subsequent experiments, a vacuum pressure of 20 kPa was selected because it gave the highest degree of deformation.

3.4. Optimising keratinocyte adhesion to the PLGA membrane

To determine the optimal collagen coating concentration for the PLGA membrane, keratinocytes were seeded at a density of 75,000 cells/cm^2 on concentrations of 50 μg/ml, 100 μg/ml or 200 μg/ml bovine type I collagen and cultured in complete FAD medium for 48h. The cultures were then fixed and stained with antibodies to β1 integrin and involucrin with DAPI as a nuclear counterstain. As shown in Fig. 5A, the cells formed stratified sheets of basal (β1 integrin-positive) and suprabasal, differentiating (involucrin-positive) cells on each collagen coating. Therefore, a concentration of 50 μg/ml was selected for subsequent experiments because it was sufficient to support keratinocyte attachment.

We also evaluated the optimal plating time to allow stratified sheet formation prior to applying the vacuum (Fig. 5B). Regardless of whether cells were seeded in complete KSFM or complete FAD, the cells that adhered up to 6h were primarily β1 integrin-positive, involucrin-negative cells, consistent with our previous studies [18]. However, by 24h involucrin-positive cells were present, indicating that some cells had initiated terminal differentiation. For subsequent experiments, cells were seeded overnight in KSFM and then transferred to complete FAD medium at the time when the vacuum was applied.

3.5. Stem cell patterning on dynamic topographies

After 48h of applying a constant 20 kPa vacuum pressure, PLGA membranes were recovered from the rig and the attached cells were fixed, immunostained and examined by confocal microscopy. Although the pressure had been removed, the position of the indentations, corresponding to the holes in the template, was readily observed (Fig. 6). By drawing a line

through the centre of each hole we could quantitate integrin and involucrin expression relative to the topographies on the basis of pixel intensity (y axis) per unit length (x axis). On all three topographies, β1 integrin bright cells clustered in the holes, but in contrast patterning of involucrin-positive cells was not observed. Topography 3 (Fig. 6C) differed from topographies 1 (Fig. 6A) and 2 (Fig. 6B) in that there was a ring of integrin-bright cells at the periphery of each hole, rather than a uniform distribution of integrin-bright cells across the entire hole diameter. There was no clustering of β1 integrin bright or involucrin-positive cells on the flat membrane controls. To compare the total fluorescence signal in individual indented versus flat regions of the same topographical feature, pixel intensity per unit area was measured. We quantitated 3 indented and 3 flat regions per well in a total of 3 wells per topography. On all three topographies the fluorescence intensity in the indentations was significantly higher than in the flat regions (Fig. 6).

3.6. Role of intercellular adhesion in stem cell patterning

We have previously observed that the YAP/TAZ pathway is activated in stem cell clusters on undulating PDMS topographies, as evidenced by nuclear accumulation of YAP [23]. On the PDMS substrates, YAP activation is dependent on intercellular adhesion and can be prevented by pharmacological inhibition of Rho kinase. This prompted us to examine the localisation of E-cadherin and YAP in cells on the dynamic substrates (Fig. 7).

Immunostaining showed that in the indentations of all three topographies, YAP localised to the cell nucleus, whereas elsewhere most cells had cytoplasmic YAP. As in the case of β1 integrin-bright cells (Fig. 6), the cells with nuclear YAP on Topography 3 formed a ring at the periphery of each feature (Fig. 7). E-Cadherin immunostaining was clustered in the invaginations on the topographies (Fig. 7). Treatment with the Rho kinase inhibitor Y-27632 (Enzo ALX-270-333; 10μM) at the start of application of vacuum pressure prevented the patterning of E-cadherin and nuclear YAP (Fig. 8).

4. Discussion

Here we describe the creation of a rig in which dynamic undulations of the epidermal-dermal junction can be created as a platform to study changes in the skin with age and disease. It was first reported over 20 years ago that stem cells in adult human epidermis are patterned with respect to the undulations of the epidermal-dermal junction [24]. However, until recently the underlying mechanisms were unclear. The clustering of integrin-bright keratinocytes on the

tips of PDMS substrates that mimic the topography of healthy young skin (feature diameter of 150 μm and centre-to-centre distance of 100 μm) [18] indicated that clustering is not dependent on the presence of other cell types, such as fibroblasts or vascular endothelial cells. This is also consistent with the finding that keratinocytes can spontaneously organise into clusters when cultured on a flat substrate [24]. We have also shown that clustering is dependent on intercellular adhesion and can be disrupted by inhibiting Rho kinase signalling or the non-muscle myosin II inhibitor Blebbistatin [23].

Our observations with the dynamic rig are largely consistent with the earlier studies on static PDMS substrates [18], specifically that clustering can be achieved based on topography and that it is dependent on Rho kinase activity. However, it also provides new insights into the process. First, we show that topographical features can impose patterning on a flat sheet of cells, and that the reorganisation occurs within 48h. Secondly, although *in vivo* lineage tracing in mouse skin has established that differentiating cells tend to be the progeny of basal layer cells that lie directly beneath them [25], we found that stem cell clustering can be induced independent of the location of differentiating, involucrin-positive cells. This is consistent with the finding that differentiating cells can move relative to underlying basal cells, for example during wound healing [26–28].

One surprising finding was that integrin-bright clusters formed in the indentations, rather than the tips, of the features of dynamic substrates. This is the opposite orientation to that found on static topographies [18]. However, it is in agreement with the observation that in some body sites stem cells are located in the rete ridges [24,29] and suggests that it is the undulations rather than their direction, that is important. We also noted that on Topography 3, which has the largest diameter holes, the integrin bright cells with nuclear YAP formed a rig at the edge of the holes rather than being uniformly distributed. This suggests that local forces at the edge of the features are most important, and correlate with the organisation of intercellular adhesions [30–32]. Crowding in the epidermal basal layer is known to affect cell shape and play a role in triggering exit into the suprabasal layer through a decrease in cortical tension and increased cell-cell adhesion [30]. We envision that future modifications to the rig to allow live imaging may reveal whether or not the cells in the centre of Topography 3 are more likely to differentiate that cells are the periphery [23].

5. Conclusions

We have designed, developed and optimised a novel device that provides a better understanding of how stem cell behaviour is influenced by the topography of the epidermal-dermal junction. The specific regions where stem cells are located can be controlled in a dynamic model that allows us to simultaneously mimic different topographical features by applying vacuum pressure through a rig.

6. Acknowledgements

We are very grateful to the following people for their assistance: Dr Katie Bardsley from the Institute for Science & Technology in Medicine, Keele University; Dave Pearsall from the Workshop of the Royal Stoke University Hospital; Dr Nadeem Rizvi from Laser Micromachining Ltd; and William Luckhurst and Luke Barton from the Physics Department of King's College London. FMW is very grateful to the BBSRC (grant number BB/M007219/1), MRC (MR/K026666/1) and Wellcome Trust (096540/Z/11/Z) for funding.

Data availability

The raw/processed data required to reproduce these findings cannot be shared at this time due to technical or time limitations.

7. References

[1] Watt FM. Mammalian skin cell biology: at the interface between laboratory and clinic. Science 2014;346:937–40. doi:10.1126/science.1253734.

[2] Briggaman RA, Wheeler CE. The Epidermal-Dermal Junction. J Invest Dermatol 1975;65:71–84. doi:10.1111/1523-1747.ep12598050.

[3] Cevenini E, Invidia L, Lescai F, Salvioli S, Tieri P, Castellani G, et al. Human models of aging and longevity. Expert Opin Biol Ther 2008;8:1393–405. doi:10.1517/14712598.8.9.1393.

[4] Zouboulis CC, Adjaye J, Akamatsu H, Moe-Behrens G, Niemann C. Human skin stem cells and the ageing process. Exp Gerontol 2008;43:986–97. doi:10.1016/j.exger.2008.09.001.

[5] Giangreco A, Goldie SJ, Failla V, Saintigny G, Watt FM. Human Skin Aging Is

Associated with Reduced Expression of the Stem Cell Markers β1 Integrin and MCSP. J Invest Dermatol 2010;130:604–8. doi:10.1038/jid.2009.297.

[6] Lemini-López A, Flores-Romo L, Arévalo-López A, Meza I. Altered morphology and distribution of cellular junction proteins in non-lesional psoriatic epidermis: An insight into disease severity. Arch Med Res 2006;37:36–44. doi:10.1016/j.arcmed.2005.07.003.

[7] Murphy M, Kerr P, Grant-Kels JM. The histopathologic spectrum of psoriasis. Clin Dermatol 2007;25:524–8. doi:10.1016/j.clindermatol.2007.08.005.

[8] Burgeson RE, Christiano AM. The dermal-epidermal junction. Curr Opin Cell Biol 1997;9:651–8. doi:10.1016/S0955-0674(97)80118-4.

[9] Jensen UB, Lowell S, Watt FM. The spatial relationship between stem cells and their progeny in the basal layer of human epidermis: a new view based on whole-mount labelling and lineage analysis. Development 1999;126:2409–18.

[10] Ghazizadeh S, Taichman LB. Organization of stem cells and their progeny in human epidermis. J Invest Dermatol 2005;124:367–72. doi:10.1111/j.0022-202X.2004.23599.x.

[11] Potten CS, Booth C. Keratinocyte stem cells: A commentary. J Invest Dermatol 2002;119:888–99. doi:10.1046/j.1523-1747.2002.00020.x.

[12] Webb A, Li A, Kaur P. Location and phenotype of human adult keratinocyte stem cells of the skin. Differentiation 2004;72:387–95. doi:10.1111/j.1432-0436.2004.07208005.x.

[13] Watt FM, Hogan BL. Out of Eden: stem cells and their niches. Science 2000;287:1427–30. doi:10.1126/science.287.5457.1427.

[14] Bellas E, Seiberg M, Garlick J, Kaplan DL. *In vitro* 3D Full-Thickness Skin-Equivalent Tissue Model Using Silk and Collagen Biomaterials. Macromol Biosci 2012;12:1627–36. doi:10.1002/mabi.201200262.

[15] Van Der Veen VC, Boekema BKHL, Ulrich MMW, Middelkoop E. New dermal substitutes. Wound Repair Regen 2011;19. doi:10.1111/j.1524-475X.2011.00713.x.

[16] Gibot L, Galbraith T, Huot J, Auger F a. A preexisting microvascular network benefits *in vivo* revascularization of a microvascularized tissue-engineered skin substitute. Tissue Eng Part A 2010;16:3199–206. doi:10.1089/ten.tea.2010.0189.

[17] Pereira RF, Sousa A, Barrias CC, Bayat A, Granja PL, Bártolo PJ. Advances in bioprinted cell-laden hydrogels for skin tissue engineering. Biomanufacturing Rev 2017;2:1. doi:10.1007/s40898-017-0003-8.

[18] Viswanathan P, Guvendiren M, Chua W, Telerman SB, Liakath-Ali K, Burdick JA, et al. Mimicking the topography of the epidermal–dermal interface with elastomer substrates. Integr Biol 2016;8:21–9. doi:10.1039/C5IB00238A.

[19] Clement AL, Moutinho TJ, Pins GD. Micropatterned dermal-epidermal regeneration matrices create functional niches that enhance epidermal morphogenesis. Acta Biomater 2013;9:9474–84. doi:10.1016/j.actbio.2013.08.017.

[20] Bush K a, Pins GD. Development of microfabricated dermal epidermal regenerative matrices to evaluate the role of cellular microenvironments on epidermal morphogenesis. Tissue Eng Part A 2012;18:2343–53. doi:10.1089/ten.TEA.2011.0479.

[21] Sahoo SK, Panda AK, Labhasetwar V. Characterization of porous PLGA/PLA microparticles as a scaffold for three dimensional growth of breast cancer cells. Biomacromolecules 2005;6:1132–9. doi:10.1021/bm0492632.

[22] Yang Y, El Haj AJ. Biodegradable scaffolds - delivery systems for cell therapies. Expert Opin Biol Ther 2006;6:485–498 ST–Biodegradable scaffolds–delivery s. doi:10.1517/14712598.6.5.485.

[23] Walko G, Woodhouse S, Pisco AO, Rognoni E, Liakath-Ali K, Lichtenberger BM, et al. A genome-wide screen identifies YAP/WBP2 interplay conferring growth advantage on human epidermal stem cells. Nat Commun 2017;8:1–16. doi:10.1038/ncomms14744.

[24] Jones PH, Harper S, Watt FM, Le L. Stem Cell Patterning and Fate in Human Epidermis 1995;80:83–93.

[25] Clayton E, Doupé DP, Klein AM, Winton DJ, Simons BD, Jones PH. A single type of progenitor cell maintains normal epidermis. Nature 2007;446:185–9.

doi:10.1038/nature05574.

[26] Headon D. Reversing stratification during wound healing. Nat Cell Biol 2017;19:595–7. doi:10.1038/ncb3545.

[27] Aragona M, Dekoninck S, Rulands S, Lenglez S, Mascré G, Simons BD, et al. Defining stem cell dynamics and migration during wound healing in mouse skin epidermis. Nat Commun 2017;8. doi:10.1038/ncomms14684.

[28] Donati G, Rognoni E, Hiratsuka T, Liakath-Ali K, Hoste E, Kar G, et al. Wounding induces dedifferentiation of epidermal Gata6 + cells and acquisition of stem cell properties. Nat Cell Biol 2017;19:603–13. doi:10.1038/ncb3532.

[29] Lavker R, Sun T. Heterogeneity in epidermal basal keratinocytes: morphological and functional correlations. Science (80-) 1982;215:1239–41. doi:10.1126/science.7058342.

[30] Miroshnikova YA, Le HQ, Schneider D, Thalheim T, Rübsam M, Bremicker N, et al. Adhesion forces and cortical tension couple cell proliferation and differentiation to drive epidermal stratification. Nat Cell Biol 2017;20. doi:10.1038/s41556-017-0005-z.

[31] Rübsam M, Mertz AF, Kubo A, Marg S, Jüngst C, Goranci-Buzhala G, et al. E-cadherin integrates mechanotransduction and EGFR signaling to control junctional tissue polarization and tight junction positioning. Nat Commun 2017;8:1–15. doi:10.1038/s41467-017-01170-7.

[32] Mertz AF, Che Y, Banerjee S, Goldstein JM, Rosowski K a, Revilla SF. Epithelial Cell – Matrix Traction Forces. Proc Natl Acad Sci 2013;110:842–7. doi:10.1073/pnas.1217279110/-/DCSupplemental.www.pnas.org/cgi/doi/10.1073/pnas.1217279110.

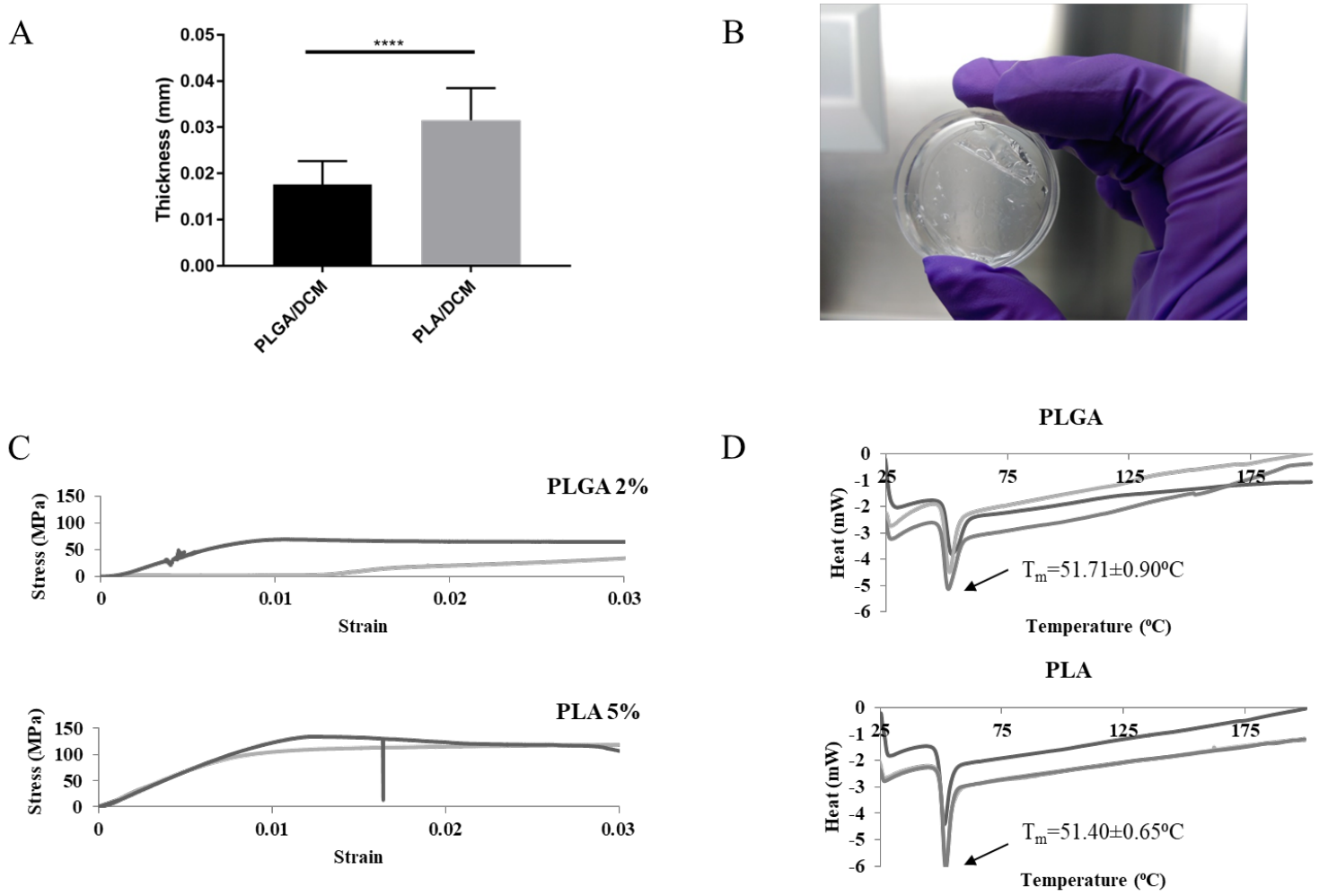

Figure 1.Membrane characterization (A) Thickness of 2% (w/v) PLGA and 5 % (w/v) PLA dissolved in DCM using the same volume of solvent. ****P ≤ 0.0001. (B) Representative photograph showing transparency of the PLGA membrane. (C) Mechanical characterization using uniaxial tensile test of PLGA and PLA. (D) Differential Scanning Calorimeter (DSC) test of 2% (w/v) PLGA and 5 % (w/v) PLA to determine the melting point of each polymer. Three samples of each polymer were analysed.

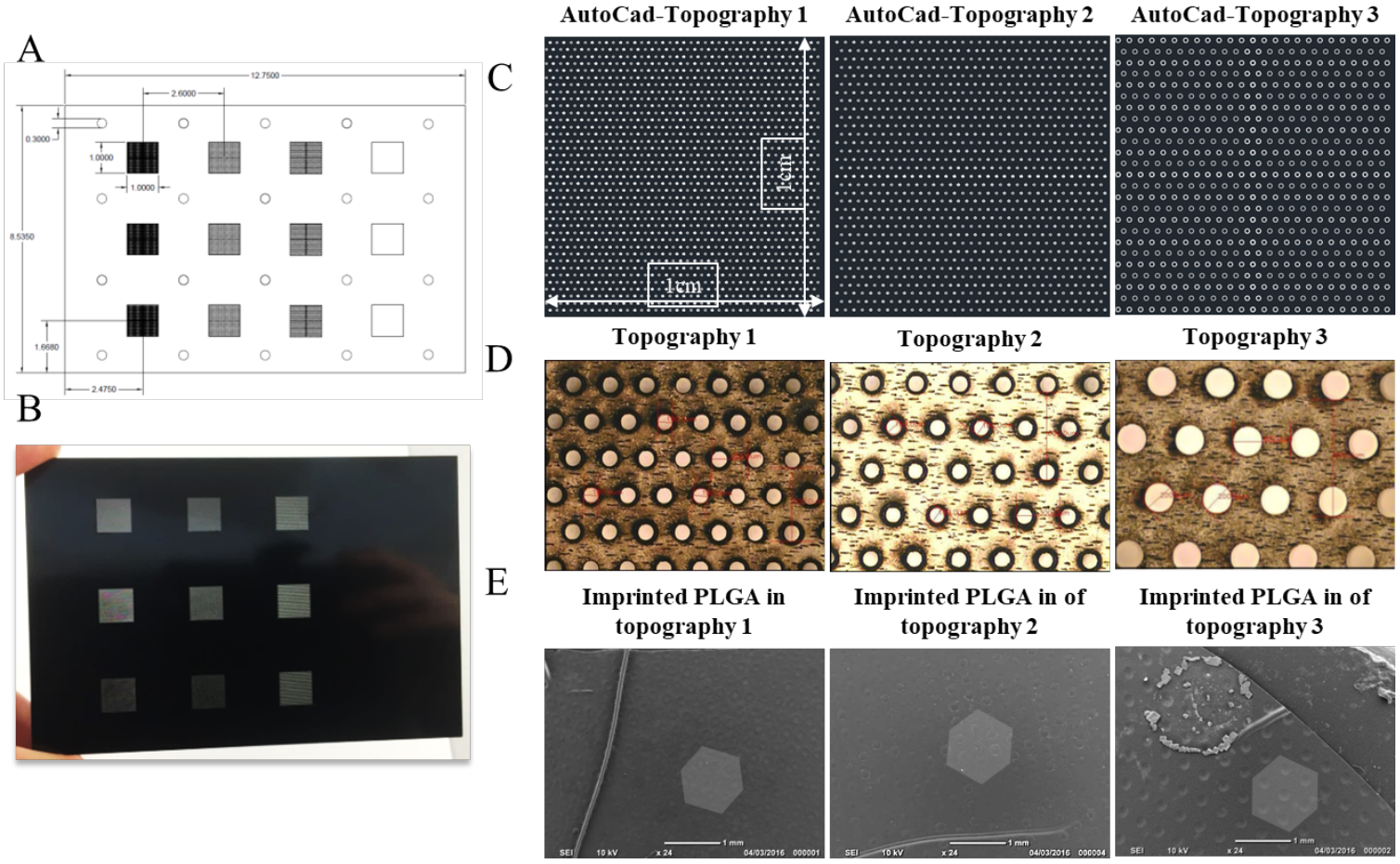

Figure 2.Template design and characterization (A) Design of the template in AutoCad. (B) template produced in a 500µm thick polyimide sheet. (C, D) Light microscopy of each topography in the polyimide sheet, showing diameter and spacing of holes. (E) SEM images of PLGA membrane placed on top of the topographies after applying 20 kPa vacuum pressure for 30 min.

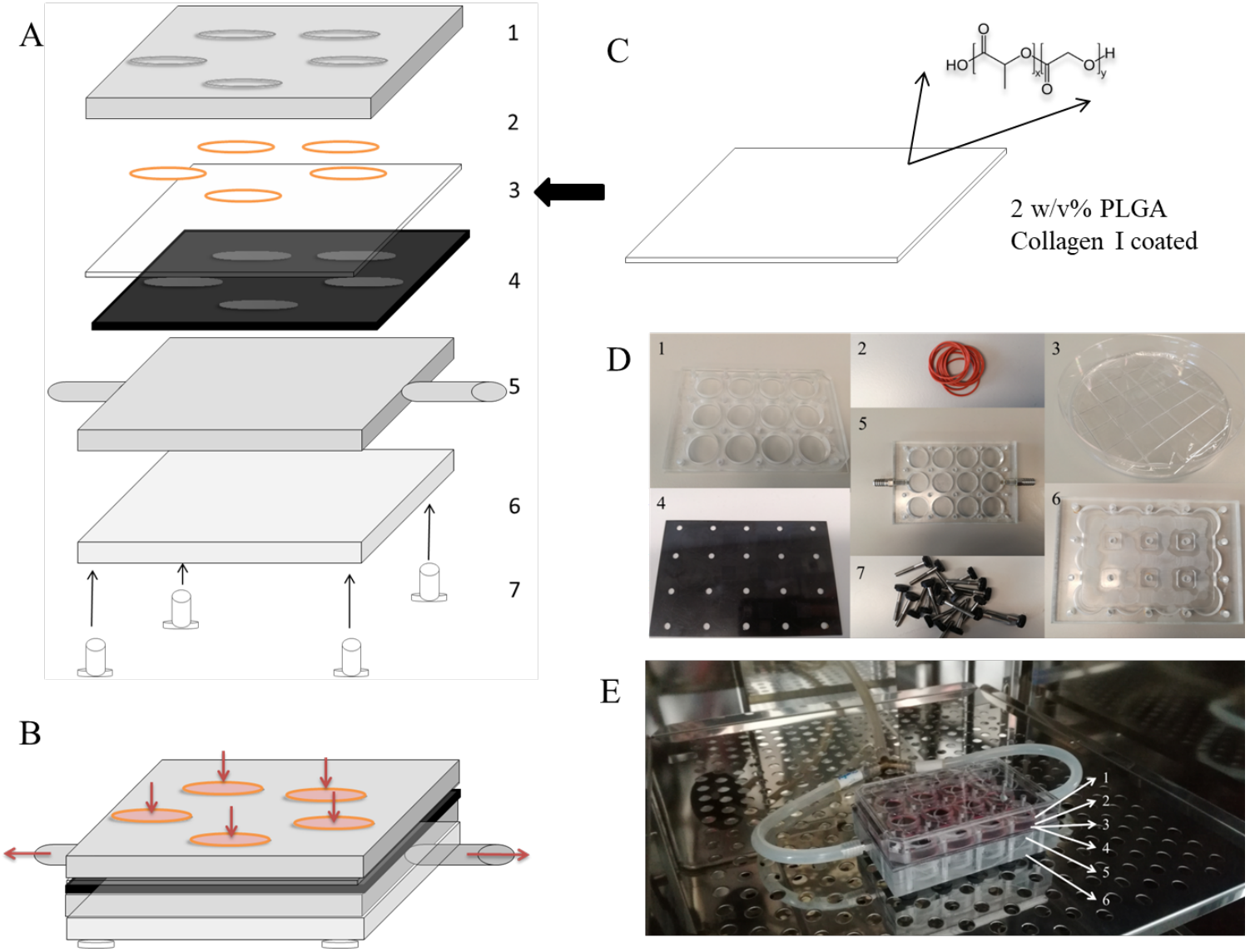

Figure 3. Schematic diagram of rig-template-membrane assembling (A) The polyimide template (4) is placed on top of that part of the rig with the outlets to the vacuum pump (5). The PLGA membrane (3) is placed on top of the template and is deformed when vacuum suction is applied (B). The other components of the assembly (A) are shown in (D). (C) PLGA is pre-coated with Collagen I prior to assembly of the rig. (E) The different components (A, D) in an incubator following assembly.

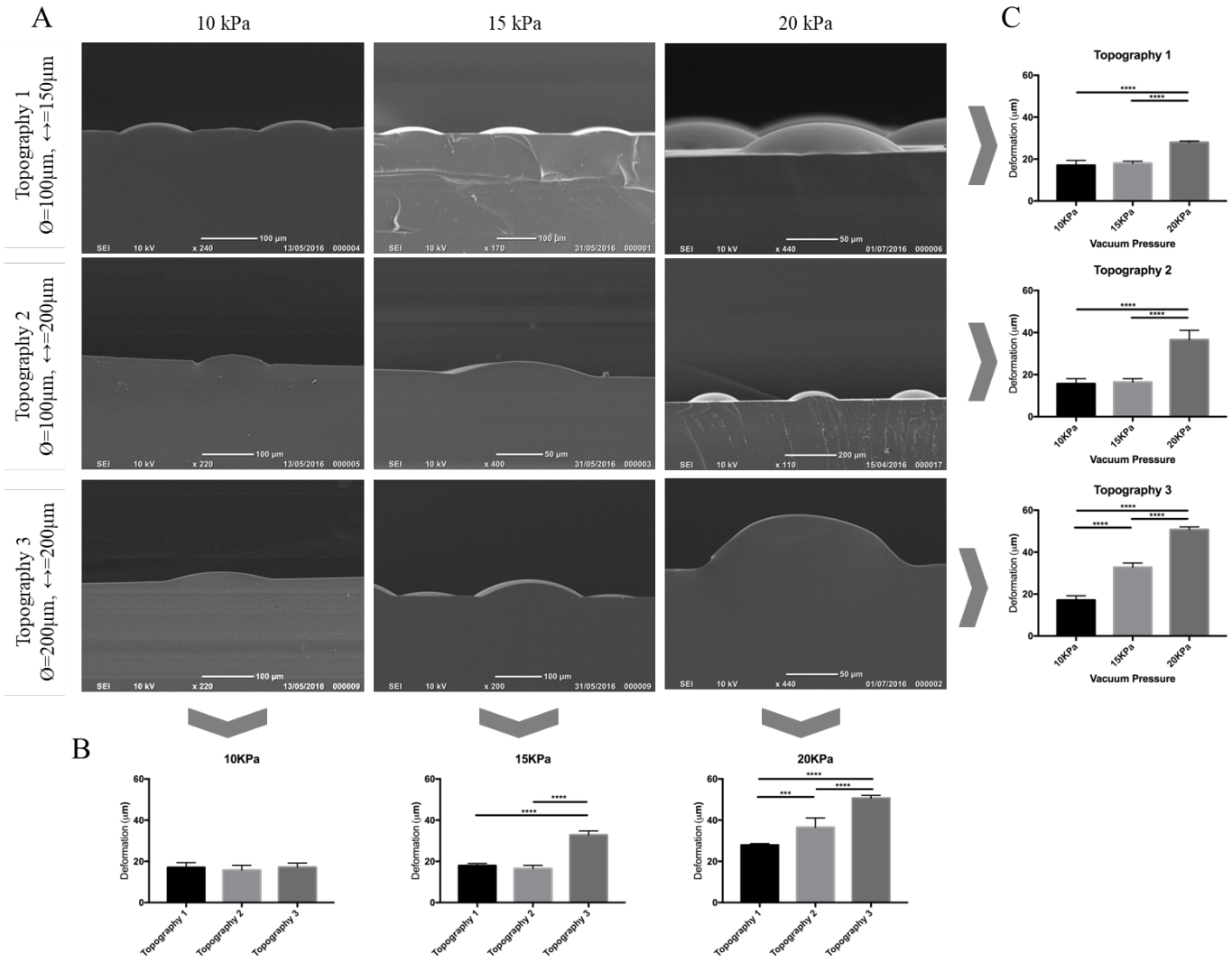

Figure 4. Vacuum-induced indentations. (A) SEM of PDMS stamp showing PLGA deformation by vacuum pressure. (B, C) ImageJ was used to quantitate deformation as a function of topography (B) and vacuum pressure (C). n = 3 images per sample; n = 3 samples for each condition. ****P ≤ 0.0001; ***P < 0.001.

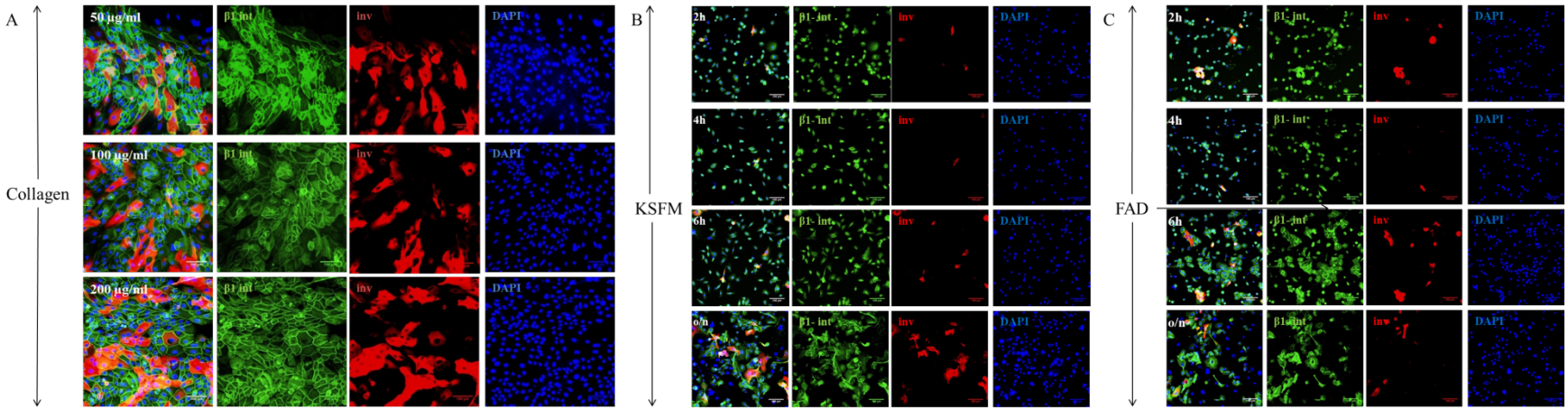

Figure 5. Cell adhesion on flat PLGA. (A) Effect of different collagen coating concentrations. PLGA was coated with 50, 100 or 200 µg/ml Collagen type I and keratinocytes were seeded at a density of 75,000 cell/cm^2 for 48 hours in FAD medium. **(B, C) Effect of different culture media.** Keratinocytes were seeded at a density of 75,000 cell/cm^2 in KSFM (B) or FAD medium (C) for the number of hours shown. (A-C) Cells were fixed and labelled with antibodies to involucrin (red), β1 integrin (green) and DAPI as a nuclear counterstain (blue).

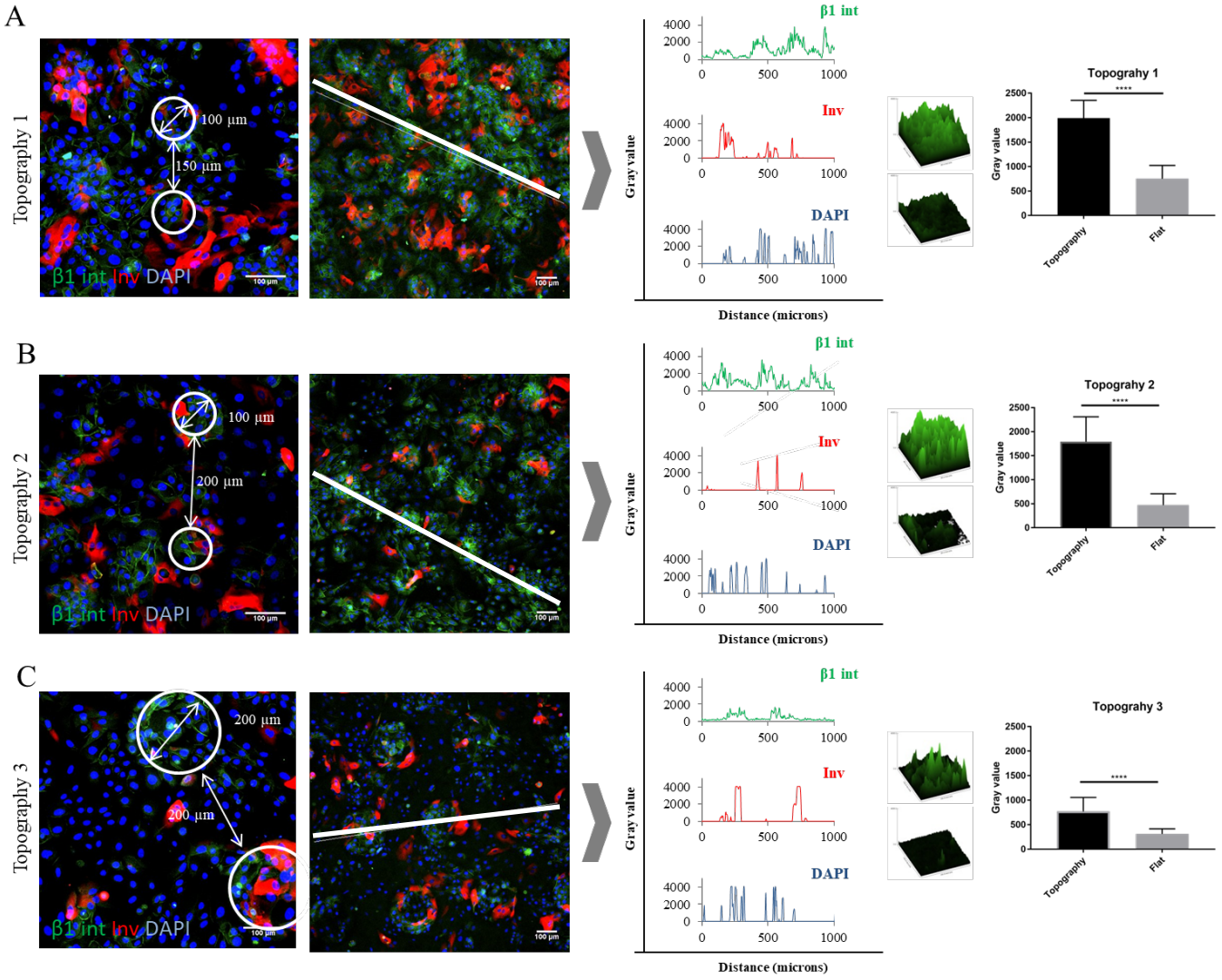

Figure 6. **Effect of topographies on involucrin and β1 integrin expression after culture under vacuum for 48h.** Cells were fixed and labelled with antibodies to involucrin (red), β1 integrin (green) and DAPI as a nuclear counterstain (blue). Left to right: representative high magnification images showing spacing of holes (circled); lower magnification views showing lines drawn through the centre of adjacent holes; corresponding pixel intensities; β1 pixel intensity per indented versus flat area. Histograms showing pixel intensity per 120 pixels total for topographies 1 and 2 (equivalent to 100 µm x 100 µm area) and 240 pixels total for topography 3 (equivalent to 200 µm x 200 µm area) n = 3 flat and 3 indented regions per membrane, and 3 membranes. ****P ≤ 0.0001.

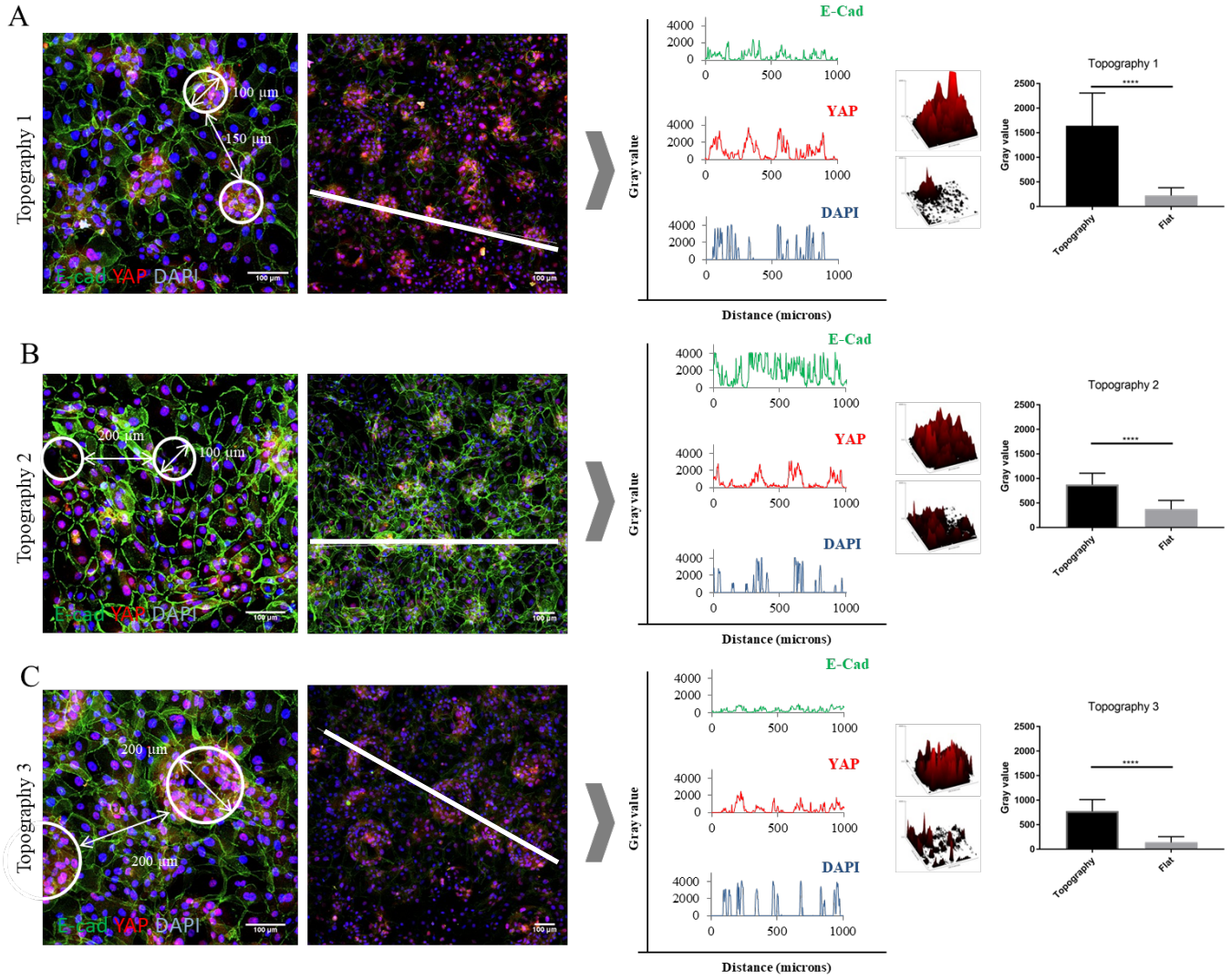

Figure 7. **Effect of topographies on YAP and E-cadherin expression after culture under vacuum for 48h.** Cells were fixed and labelled with antibodies to YAP (red), E-cadherin(green) and DAPI as a nuclear counterstain (blue). Left to right: representative high magnification images showing spacing of holes (circled); lower magnification views showing lines drawn through the centre of adjacent holes; corresponding pixel intensities; YAP pixel intensity per indented versus flat area. Histograms showing pixel intensity per 120 pixels total for topographies 1 and 2 (equivalent to 100 µm x 100 µm area) and 240 pixels total for topography 3 (equivalent to 200 µm x 200 µm area) n = 3 flat and 3 indented regions per membrane, and 3 membranes. ****$P \leq 0.0001$.

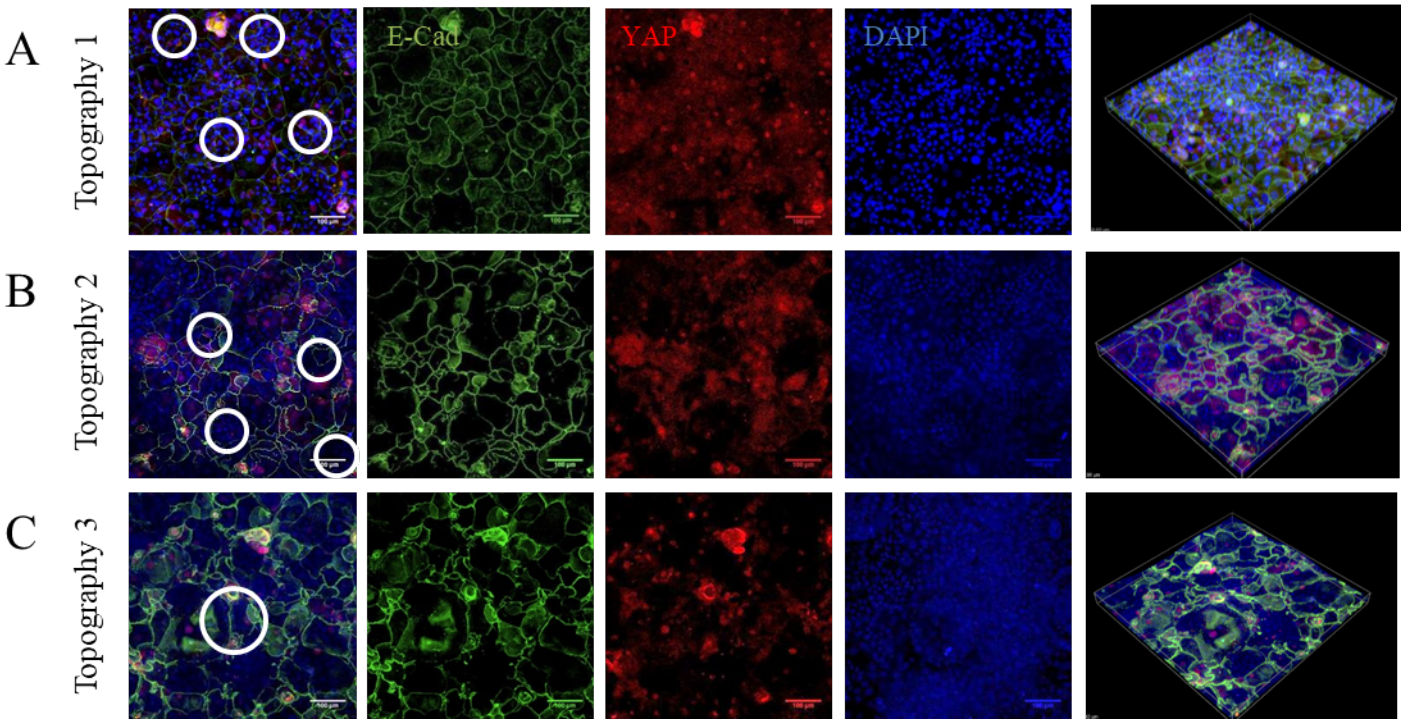

Figure 8. Effect of Rho kinase inhibition on YAP and E-Cadherin expression. Representative images of topographies 1 (A), 2 (B) and 3 (C) after culturing keratinocytes for 48 hours under vacuum pressure in FAD medium containing ROCK inhibitor. Cells were fixed and labelled with antibodies to YAP (red), E-cadherin (green) and DAPI as a nuclear counterstain (blue). Individual confocal images and Z-stacks (right hand side) are shown.